Optimization and Performance of the STIMT Technique at the Nuclear Microprobe of IST/CTN

Manuel Couceiro Beleza Guimarães Fortunato
manuel.fortunato@tecnico.ulisboa.pt

Instituto Superior Técnico, Lisboa, Portugal

October 2020

Abstract

In a previous research project STIM tomography had already been proved to be possible to perform with the nuclear microprobe of IST/CTN. However the practical use of this technique was not yet assured since the rotation of the sample, which is done with a stepper motor, was not automatized which meant that the operator repeatedly had to intervene in the process making it longer and more prone to errors. In the present work the equipment for tomography was once again set into operation and the acquisition process was completely automatized through the inclusion of the command of the stepper motor in the software that is used for the command of the remaining aspects of the acquisitions in the microprobe, OMDAQ. The system was validated by the acquisition and reconstruction of real data that resulted from the analysis of a human hair. The reconstruction software used was assessed through the reconstruction of simulated data.

Keywords: automation, microprobe, ion beam, tomography.

1. Introduction

It has been shown that it is possible to execute STIM and PIXE tomography with the nuclear microprobe present at the "Campus Tecnológico e Nuclear" (CTN) of Instituto Superior Técnico. The research project in which the proper equipment and expertises for doing so were developed ended in 2015. All its information can be seen in [1]. The acquired/developed instruments include a gaseous detector and the associated tools for the gas flow, 2 motors for the positioning of the sample, a goniometer with 6 degrees of freedom to ensure an adequate rotation of the sample and custom made parts that are inserted in the target chamber to support the remaining equipment that is inserted. In order to perform once again STIMT at CTN it is necessary to evaluate the operational status of these instruments.

The hardware that composes CTN's nuclear microprobe is mainly made by Oxford Microbeams. For acquisition and processing of data a specialized software that is suitable for the equipment used is needed. OMDAQ, also made by Oxford Microbeams, is the software that is used for the control of the microprobe and for some processing of the data acquired. Despite the successful proof of concept, up to now STIMT was not an easy task to perform at CTN since the experimental procedure was not fully automated. A second software (besides OMDAQ) was necessary to control the motor that performs the rotation of the sample. This meant that every time the sample had to be moved to a new angular position the operator would have to intervene. For a high number of angular positions, which can be greater than 100 for a greater precision in the reconstruction, the process became very slow and completely impractical. A goal for the present work is to solve this problem by integrating the command of the rotation motor in the OMDAQ software. The procedure then becomes fully automated and (if everything goes right) only a set of acquisition parameters and commands must be defined at the beggining, no further action by the operator being needed. This makes the procedure faster, more reliable and easier to execute and is necessary so that STIMT can be used at CTN.

The main objective of the present work is to assure that STIMT is a technique that can be easily used at CTN. Naturally its success is validated through the execution of a full STIMT experiment, from the acquisition of projections to the reconstruction of the final 3D image of the sample. The used reconstruction software was assessed through the use of simulated projections from a phantom created specifically for this purpose.

2. Background

2.1 Data acquisition

STIMT was performed with the nuclear microprobe which is installed at the 2.5 MV Van de Graaff accelerator of IST/CTN.

The protons are detected by a gas detector developed specifically for STIM. By operating in pulse mode, the pulse induced by each individual incident particle is measured independently. It uses a mixture of He and $HC(CH_3)_3$ (isobutane). Unlike the traditional PIN diodes used for STIM it does not suffer from radiation damage since the detection medium's purity inside the chamber is always assured. In [2] its response to 2 MeV H^+ and He^+ was studied and the minimum energy resolution obtained was of 26 keV. This is a similar value to the energy resolution of the traditionally used Si PIN diodes in the same working conditions which is in the range of 15 to 30 keV.

If a proton is detected in the gas detector a pulse is generated that is processed by the acquisition electronics and converted to digital by the 12 bit ADC (Analog-to-Digital Converter) used. The signal of several detected protons is presented by OMDAQ in the form of a spectrum and of one or several two dimensional maps. These maps have a resolution of 256×256 pixels when the scan is performed in internal mode[a], as is usually the case. The maps show the number of protons detected for each position of the beam with a residual energy that is within a certain interval, chosen from the experimental spectrum. The number of counts is indicated by a color code, as is shown in figure 1.
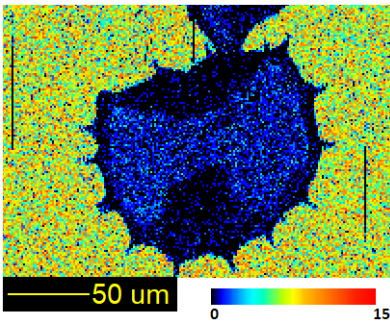

Figure 1: Transmitted proton counts in the energy interval ≈ 1871-2100 keV that result of the STIM analysis of a pollen grain with a ≈2 MeV beam with the nuclear microprobe at CTN.

Beside the maps and the spectra during the experimental acquisition OMDAQ stores in the computer a file with information about every detection made. For each detection it stores a matrix entry which comprises the source (one of the eight analog entries available in the ADC), the (two) coordinates for the position of the beam and the energy. This format, called "list mode" or "event-by-event", has the information needed for the reconstruction process. From the generated file the experimental data can be converted into a format that is readable by the preprocessing software.

2.2 Automation

The initial situation found, before the present work took place, was the following:

1. Software

   (a) the software used for the command and control of the microprobe, called OMDAQ98, does not allow for the command of external hardware. Also it is meant to be used with Windows98 which is an outdated operating system.

   (b) there are two newer versions of the OMDAQ software, which are called OMDAQ 2007 and OMDAQ-3, that can be used to command and control the microprobe. Both can, in principle, command one (or several) external motor(s) if the appropriate code is used.

   (c) using the more recents versions of the OMDAQ software requires:

      i. exchanging part of the hardware used by new hardware (point 2a);

      ii. writing and providing the code for the command of the rotation motor;

      iii. operational tests;

2. Hardware

   (a) the interface between the computer and the microprobe's hardware is done with two cards for digital input/output. In order to use the newer versions of OMDAQ (2007 or 3) to command and control the microprobe newer cards have to be installed. The operating system of the computer used must be either WindowsXP for OMDAQ 2007 or Windows7 or 10 for OMDAQ-3.

   (b) when data is being acquired during a tomography experiment the current that flows to the stepper motor is suppressed with a manual switch in order to reduce the electronic noise in the detection system. This solution is not compatible with automatic execution.

OMDAQ performs an automated procedure by executing in sequence several programmed runs. A programmed run stores the following information:

---

[a]In this mode the voltage levels that indicate the beam position are created by a card with an 8 bit DAC installed in the computer and therefore are discretized in 256 values.

title of the operation, the scanning parameters, the sample's position and the preset stopping conditions. Each programmed run is executed by moving the stage to the defined position, loading the scan parameters and executing the scan until the preset stop conditions are reached.

The scanning parameters define the scanning pattern and how each pixel is irradiated. For 3D tomography the scan can be made along a 2D square grid, usually of 256×256 pixels, with the option "full 2d scan" or along the area defined by a drawing in a map with the option "selected raster". The latter option can save a lot of time by discarding the areas of the maps where the sample is not present. For each irradiated pixel a set of criteria must be fulfilled before the beam moves to the next pixel. These pixel clocking conditions are usually a given number of events detected in an energy interval that discards the low energy electronic noise and the high energy pile up. Each programmed run produces a list mode file with the information of every data pulse recorded by the data acquisition system.

2.2.1 The hardware

The motor used for the rotation of the sample is a high vacuum Phytron VSS32.200.1.2. It is a two-phase bipolar hybrid stepper motor of 200 steps per revolution prepaired to operate in a vacuum with a pressure as low as 10^{-7} mbar. When used in quarter-step mode it has an angular precision of 0.45°. For its command it was connected to a driver board (MSE570-2 RS Components) for bipolar stepper motors and to a programmable board (V8849 RS Components) that allows the command of up to 2 stepper motors through their driver boards. The communication with the programmable board is done through a RS-232 protocol and the programming is done with a language similar to C.

2.2.2 Electronic noise

A problem that must be solved in order to successfully automate the STIMT data acquisition procedure is the presence of eletronic noise. Stepper motors are usually energized when standing still in order to activate their holding torque and assure that there are no deviations from the intended position. However if the motor used is energized inside the vacuum chamber when data is acquired there will be a great amount of electromagnetic noise in the detection system due to the flowing current. The noise signals in the microprobe detection system are typically below 300 mV in the 0 V to 10 V range of the ADC used. The noise that results from the stepper motor is about 10 times greater going up to 3 V, making impossible the acquisition of data.

Since the common techniques of filtering and shielding were not efficient in reducing the noise, in previous tomography experiments the current flow was suppressed by a switch acted manually.

2.3 JPIXET

JPIXET is a preprocessing, simulation and reconstruction software for PIXET, written in JAVA at CTN [3]. It was mainly written to accelerate iterative PIXET reconstruction methods using GPUs ("Graphics Processing Units") and CUDA (*"Compute Unified Device Architecture")* libraries. It possesses an accelerated version of the MLEM (*"Maximum Likelihood Expectation Maximization"*) algorithm and of the DISRA [4] (*"Discretized Image Space Reconstruction Algorithm"*). Although, regarding DISRA, it can only perform the PIXE (accelerated) simulations and, optionally, perform the (accelerated) FBP (*"Filtered Backprojection"*) on the PIXE data, making use of the DisraSlice software for all the STIMT simulations and reconstructions[b]. To evaluate the capabilities and limitations of the simulations and of the reconstruction techniques, JPIXET is able to perform the simulation of PIXET experiments on phantoms - objects, in this case software created, for evaluating, analyzing and tuning of the imaging equipment. The result of such simulations is a set of projections of energy loss measurements (STIM) and x-ray counts (PIXE). In this case it does both the simulation of STIM and PIXE, calculating the energy losses with the stopping powers of Ziegler et al. [5].

3. Implementation
3.1 Processing experimental data

There are several experimental constraints which limit the quality of the acquired data. Regarding the protons' physics there is transverse straggling and energy straggling. Transverse straggling corresponds to the increasing transverse spread of the protons of the beam as they travel deeper into the sample. The energy straggling corresponds to the uncertainty in the amount of energy a proton looses when traveling through the sample due to the statistical variations in the scattering processes. Regarding the detection system, some of the events detected experimentally are actually low energy electronic noise and high energy pile up events. Lastly, the theory of tomography requires that the rotation axis is still and completely orthogonal to the reconstructed planes during rotation, which is approximated but not strictly true experimentally. To alleviate the effect of these constraints the experimental data is preprocessed, in the form of projections and sinograms. In the present work

---

[b]The PIXET technique requires that tomography with PIXE and STIM data are both done at the same time.

TomoRebuild [6] was used for this purpose. This is a preprocessing and reconstruction software package for tomography with STIM and PIXE.

3.1.1 Correction of sinograms/projections

Counts due to electronic noise and pile up can be seen at the bottom and top of the energy spectrum, respectively, and create a random "speckle" noise in the sinograms. To avoid this a lower and an upper thresholds on the energy are provided by the user to discard the unwanted events. In a second step the data is median (or mean) filtered so that the most probable transmission energy is selected for each pixel of the sinograms. Despite filtering some spurious pixels may still be present. To eliminate these another algorithm can be applied to the data. A pixel is corrected only if it satisfies two criteria: if the number of events collected at that position is smaller than a user defined threshold and if the difference with its 2 immediate neighbours is higher than a user defined threshold. If both are verified then the pixel's value is replaced by an average of the values of its 2 neighbours. The procedure is performed considering the neighbours in the sinogram (in the same horizontal line first and afterwards in the same vertical line) and, if required, in the projection (in the same vertical line). Lastly, to eliminate the noise that remains outside of the sample, its edges in the sinograms are detected and used to create a mask. All the pixels outside this mask can be set to 0. The edges are detected through a two-dimensional search algorithm that is initiated in the pixel with the greatest energy loss, which is certainly part of the sample, and goes through every pixel until it finds a contour with a user defined minimum energy loss. This value is usually the energy resolution of the detector which is typically the maximum value of the fluctuations of energy in the background pixels.

3.2 Reconstruction

There are two main classes of reconstruction algorithms: analytical and iterative. The analytical ones are less computationally demanding. However the iterative ones are more capable of dealing with noise in the data and, in certain cases, produce tomograms with a greater spatial resolution. The most widely used analytical method is the Filtered Backprojection (FBP) algorithm which uses a 1D filter on the projection data before backprojecting (2D) it onto the image space. The choice of filter has a great effect on the final image. The algorithm's standard filter is the ramp filter which is very prone to noise since it favors the transmission of the higher frequencies. Other choices of filter can be useful so that the higher frequencies are suppressed and the final image is smoother. This however also blurs the contours in the image so a trade off is required according to the reconstruction's needs. The FBP algorithm is a computationally efficient and numerically stable algorithm. It was used throughout this work with the TomoRebuild software.

3.2.1 Discretized Image Space Reconstruction Algorithm

The iterative methods aim to minimize an objective function iteratively. The discretized image space reconstruction algorithm (DISRA), [4], also used for the reconstructions, is of this second type. It provides, in principle, more accurate results than the simpler FBP. After the data has been appropriately preprocessed according to what was described in 3.1, the process begins by performing the FBP on the experimental data. This reconstruction is taken as the reference one and is the first one to be used in the iteration stage of the algorithm. At each iteration a simulation of the STIM experiment is made using the tomogram obtained in the previous iteration. The projections that result of this simulation are reconstructed with the FBP. The resulting tomogram's density ρ_i is corrected by comparison with the reference reconstruction ρ_E and the result ρ_{i+1} will serve as the input for the next iteration.

Since at each iteration the FBP is performed and this algorithm amplifies noise, a scheme must be employed so that the tomogram produced after several iterations does not present large variations where the density is supposed to be constant. To prevent this effect the density values are discretized and a smoothing algorithm is used. The interval between the discrete values ΔD decreases with the iteration number so that at the first iterations where the algorithm has not converged fluctuations smaller than ΔD are prevented. The final result is that regions of nearly constant density are heavily smoothed but their boundaries are preserved.

The measure of the algorithm's success is the comparison between the simulated projections and the experimental projections. If they are close enough, then the final output is ρ_i. If not, the iterations continue. The normalized absolute error δ was used for such comparison, equation 1, where D_r is the reference data, D_t is the test data a w is the index of each pixel.

$$\delta = \frac{\sum_w |D_r(w) - D_t(w)|}{\sum_w |D_r(w)|} \quad (1)$$

The algorithm DISRA was used with the software DisraSlice which is an implementation written in

C++.

3.2.2 Number of projections

The optimal number of projections for a good reconstruction can be calculated from the lateral resolution that the projections provide. If N_w is the number of pixels of width of a rectangular window such that the sample can be fully imaged from all of the viewing angles, then the level of angular resolution in the reconstructions is optimized for a number of $\frac{\pi}{2}N_w$ projections. The demonstration can be seen in [7].

3.3 Automation

The boards necessary for using the new OMDAQ software versions - OMDAQ 2007 and OMDAQ-3 - are the Amplicon PCI-215 programmable board and the Arcom APCI-ADADIO card. The cards were tested in a computer with the operating system Windows XP and OMDAQ 2007, and in a computer with the operating system Windows 10 and OMDAQ-3. However it was later verified that the setup "Windows XP + OMDAQ 2007" was not loading the dynamic link library (DLL) created for the command of the stepper motor (more details ahead). OMDAQ-3, version 3.2.3.884, was then chosen for the execution of automated STIMT.

3.3.1 OMDAQ-3

Included in the OMDAQ-3 installation is the beginning of the source code needed to compile a dynamic link library (DLL) meant to be used by the software to command a motorized stage. This compilation was done with Embarcadero's RAD Studio 10.2 Tokyo software which provides an integrated development environment (IDE) for the creation of applications written in C++. This software was used because OMDAQ-3 was built with Embarcadero's C++ Builder "10 Seattle" and using software of the same provider made the process easier.

The auxiliary code provided by OMDAQ-3 is written in C++ and consists of two header files and a source file. One of the header files is used to define several flags that are used to inform the software of the current status and capabilities of the stage. The source file (and the corresponding header file) has several functions declared without definition. It was the definition of these functions that was projected, tested and implemented so that the command of the stepper motor could be made with OMDAQ. The most important functions are meant to:

- Report the capabilities of the stage. It returns a binary word that informs the software of what the stage can do. Each bit of the word is a flag for some capability. In the present case this function informs OMDAQ-3 that the stage can perform linear motion along the three Cartesian axis and rotation along the vertical axis because the possibility of a stage that can rotate but cannot move along all of the Cartesian axis simply was not considered in the software.

- Initialize. With the aid of a C library (available for download and described in [8]) two RS-232 communication channels are opened.

- Set the angular speed of the stage.

- Move the stage. The stage moves in 0.45° steps. It can rotate in both directions and, if the required position is greater (smaller) than the previous one, the new position is either exactly reached or approximated by default (excess).

- Obtain the current status of the stage. Through the use of bit masks defined in OmXyzDll_StatusBits.h this function modifies a 64 bit unsigned integer variable that will inform OMDAQ-3 of the current status of the stage. Amongst other information it is communicated if the stage is in movement or not, if the motors that move it are on or off and if any software defined limits for the position have been reached.

3.3.2 Electronic noise

By studying the manual of the MSE570-2 driver board it was verified that by connecting the pin 18a to the ground the current flow to the motor is suppressed. This pin is called "output disable input". This can be used to cut off the motor's power supply when the sample is under irradiation and data is collected. In order to achieve this by the action of a software command the simplest solution found was to use the voltage levels of a single pin of a second RS-232 port which are commanded through the same DLL that commands the motor. The "Data Terminal Ready" (DTR) signal was used: its state is easily changed and the voltage levels are high enough. This signal will act on a relay that will act as switch either connecting or disconnecting the pin 18a to the ground. Using a second RS-232 port was an obvious solution because at the time a RS-232 protocol had already been used successfully. The circuit designed is shown in figure 2.

3.4 Analyzed samples

STIMT was performed on a human hair. For a better comprehension of the results the structure of the human hair is briefly presented in this section. It can be seen in figure 3. The cuticle is the thin outermost layer and it is also the densest part of the
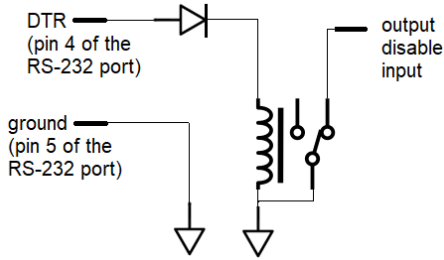
Figure 2: Circuit designed to control the supply of electric power to the stepper motor.

hair. It is made of flat overlapping cells (scales) and has usually a thickness of ≈3 to 5 μm. The cortex is responsible for the major part of the hair mass: a percentage of 70% to 90% of the total mass. It is composed of elongated cells, that can reach about 100 μm in length. The medulla usually constitutes a small fraction of the hair's mass. As a general rule the greater the diameter of the fibre the more of this tissue will be present. The morphology of the medulla is highly variable. It can be completely absent, continuous or discontinuous throughout the fiber's axis. The sample analyzed has a cross sec-
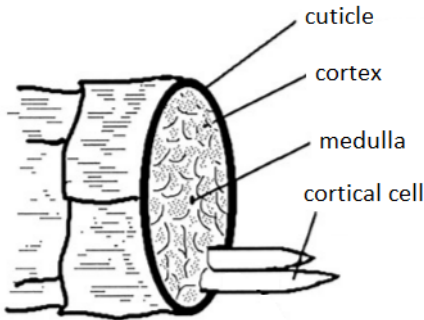

Figure 3: The basic structure of the human hair. Image adapted from [9].

tion that is approximately in the form of an ellipse with a minor axis of ≈ 49 μm and a major axis of ≈ 62 μm.

The experimental technique was also attempted with a pollen grain with an approximately spherical shape and ≈ 65 μm of radius. However due to a bug in OMDAQ-3 the data pertaining the second half (15) of the projections was not saved and therefore it was not possible to obtain a reconstruction.

3.5 JPIXET: simulations with a phantom

A specific phantom was created for the assessment and evaluation of the STIMT reconstruction software used. JPIXET simulated a PIXET experiment on this phantom and the energy loss projec-

tion data that resulted of this simulation were later reconstructed with TomoRebuild and DisraSlice.

The phantom objects are provided either through a set of tomograms or are defined internally in the JPIXET software through the "phantom" class. Since only a simple two dimensional homogeneous phantom was available the source code of the program was edited and recompiled with a new method in the "phantom" class called "makeOrgPhantom". This was done using the IDE "Apache Netbeans 11.1". The added method assigns a specific composition and set of densities to a phantom object. The experimental parameters are provided through a set of files. Most of the parameters can be changed for the present simulation. The created projections must have a width of 128 pixels and a maximum height of 128 pixels. The linear dimensions of each pixel can be changed and coincide with the beam's cross section (which is a rectangle) linear dimensions. Regarding the STIM data, the output of the simulations is a binary file with the values of energy loss, one float for each pixel.

3.5.1 Phantom

The test object created is a cylinder with 40 pixels of radius and a maximum of 128 pixels of height. It consists of several solids - spheres, ellipsoids and parallelepipeds - made out of different compounds and embedded in araldite glue. There were 4 different materials used. They are identified along with their chemical formulas and densities in table 1. The composition was chosen this way since the samples analyzed in this work (and many of the samples analyzed with STIMT in general) are biological and therefore composed mainly of the elements H, C and O. Since only 2 of the 128 reconstructed slices were actually used for the evaluation of the used software and due to the limited amount of space, the image of the phantom in 3 dimensions is not presented here. The 2 slices used, chosen for the greater complexity of their morphology, are shown in figure 4.

region	compound	formula	density (g/cm^3)
0	araldite	-	1.1
1	menadione	$C_{11}H_8O_2$	1.225
2	glicose	$C_6H_12O_6$	1.56
3	palmitic acid 13	$C_{16}H_{32}O_2$	0.852

Table 1: Composition of the phantom created with JPIXET.

4. Results
4.1 Simulations: assessing the reconstruction software
A total of 63 projections of 128×128 pixels acquired in 180° were simulated. The beam's cross section has 1 μm of width and 2 μm of height. The en-
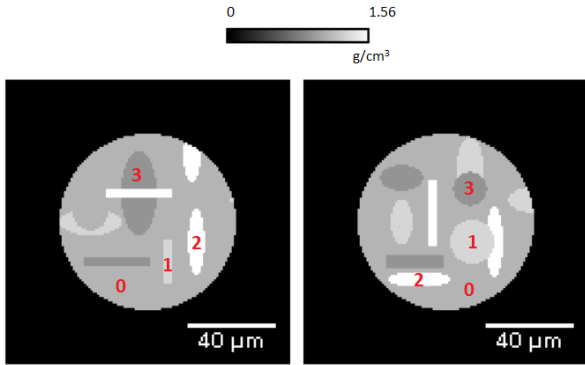
Figure 4: Slices number 26 (left) and 72 (right) of 128 total of the phantom created. The different compounds are marked with numbers according to table 1.

ergy considered was of 2.4 MeV, which is approximately the maximum energy that can be achieved with the microprobe in the lab. With these settings the minimum residual energy simulated is of $\approx$490 keV. The number of projections, 63, is half the number needed for an optimal angular resolution.

After the projections were generated, it was necessary to convert the data to the format that is required by the preprocessing software. The output format of JPIXET was converted in the input format of TomoRebuild with a script written for this purpose.

The reconstruction of 2 slices made with TomoRebuild and DisraSlice is shown in figure 5, the remaining tomograms having a similar quality. The morphology of the phantom is accurately reproduced. Both of the programs are therefore working as expected.

4.2 Hair analysis

The parameters of the experiment are shown in table 2. The number of detected events per pixel was set as 15 regardless of their energy. Due to a bug in OMDAQ-3 the energy interval could not be specified. Before an accurate reconstruction could be

ions	H^+
energy	2 MeV
number of projections	30
angular range	180º
maps resolution	256×256 pixels
height×width of scan	200 μm×200 μm
number of events per pixel	15
software	OMDAQ-3

Table 2: Parameters regarding the analysis of the hair fibre.

done, there was a problem with the projections that needed fixing. Some of them had a "hole" - a region that seems devoid of matter - in the centre of the
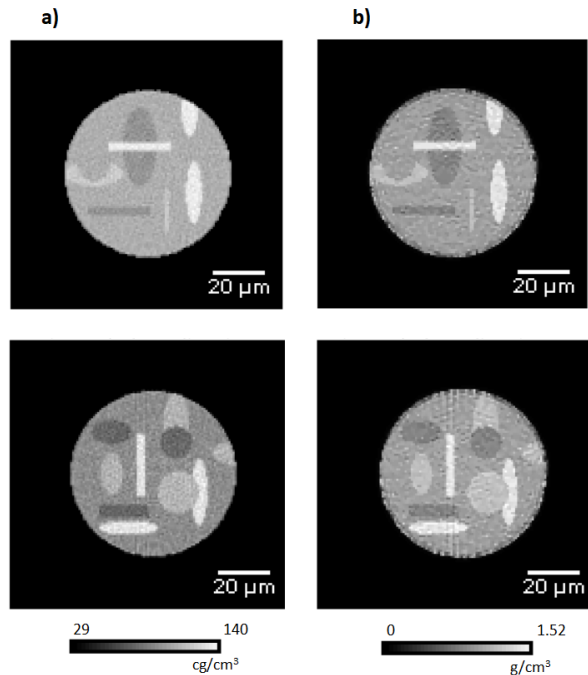

Figure 5: Reconstructions made with TomoRebuild - figure a) - and DisraSlice - figure b) - of 2 of the 128 slices of the phantom object. On top are the reconstructions of slice number 26 and on the bottom of slice number 72.

hair fibre, as can be seen in figure 6a) in which the energy loss at an angle of 162º is depicted. Compare with the projection of energy loss obtained at an angle of 72º: figure 7a). To better explain this problem the spectrum of all the events detected in the anomalous region of the projection in figure 6a), at an angle of 162º, is shown in figure 6b). The spectrum of the analogous region for the projection in figure 7a), is shown in figure 7b). In both of the spectra there is some low energy noise that was not discarded by the discriminator and a peak with a maximum of counts around 1900 keV. This corresponds to particles that lost $\approx$100 keV, which is much smaller than what is expected in the middle of the fibre - more than 1 MeV - where the beam crosses from 50 to 60 μm of hair, a great amount of matter. The peak around 1900 keV is present regardless of the detection area, and the most likely cause for it is that it results of some protons that were deflected out of the beam trajectory by scattering somewhere in the line. This created a halo or secondary beam of particles that does not cross the sample and is always detected. In the case of the projection at 162º this halo of particles was the only detection possible which means that the proper beam was not able to cross the sample or it's transmission energy was below the threshold of $\approx$330 keV of the noise discriminator. Hence only one peak is

observed in the spectrum of figure 6b) while two peaks are observed in the spectrum of figure 7b).
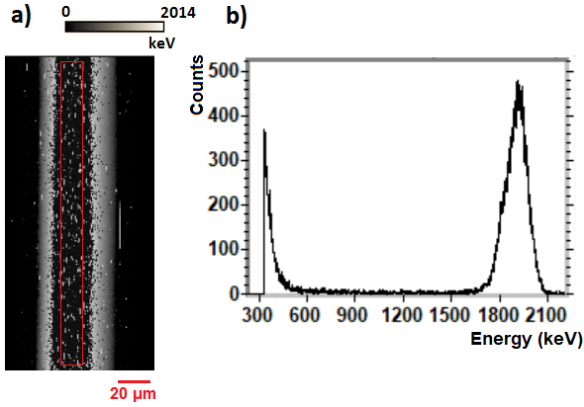

Figure 6: a) Energy loss map obtained at an angular position of 162°. b) Spectrum obtained with all the events detected in the region outlined in red in a).
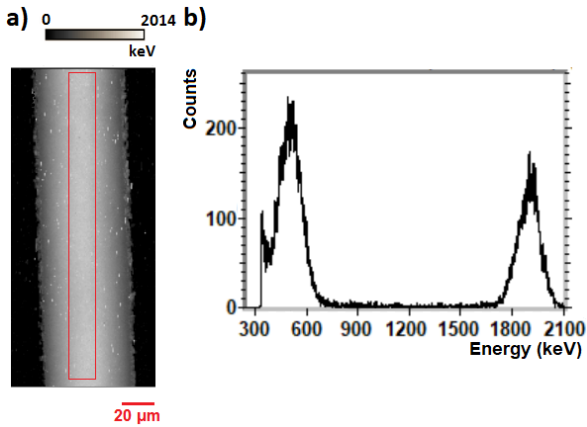

Figure 7: a) Energy loss map obtained at an angular position of 72°. b) Spectrum obtained with all the events detected in the region outlined in red in a).

In order to obtain a reasonable reconstruction the effect of the protons from the secondary beam must be removed. For this purpose the adopted strategy was to discard all of the events detected experimentally above the energy of ≈ 1640 keV, which is a value immediately below the peak that results from the anomalous events, as can be seen in the spectra in figures 6b) and 7b). This value was set as the upper energy threshold on the events when correcting the sinograms (see section 3.1.1). With this choice of threshold, naturally, there were some important events that were discarded. The ones with the greatest effect were those that resulted from the direct beam at ≈2 MeV since these were the ones that indicated the areas where no sample was present: the background. The background pixels

registered 0 events, and if no detection is present at a pixel then that means that the beam was not able to cross the sample at that point and that it lost all of it's energy. Therefore the result was that the areas that were transparent to the beam became opaque. This effect was corrected by using the edge detection function of TomoRebuild with the projections that were median filtered within the limits [330 keV, 2100 keV]. Since the direct beam energy was included in this set of projections the edges were well defined. The resulting information about the contour of the sample was used in the projections that were obtained after thresholding the energies at 1640 keV and the background pixels were restored, as is illustrated in figures 8a) and b). As it is visible there are however some pixels by the borders of the sample that were not corrected. This was alleviated by applying the algorithm for the correction of spurious pixels described in 3.1.1, as can be seen in figure 8c). The result of the correction procedure for the energy loss map obtained at an angle of 162°, in which a "hole" was visible at the center of the fibre (figure 6a)), is shown in figure 8d).

The global composition provided for the reconstructions was of 7.5% H, 46.2% C, 13.6% N, 28.3% O, 4.1% S and 0.3% Ca (mass fractions). This is a typical composition for hair . The results for one slice are in figure 9. The full volume tomograms are in figure 10. There is no visible structure. The thin outer layer that is visible in the reconstruction of figure 9a), and also partly in figure 9b), could be misleadingly identified as the cuticle. However it is actually an artifact that results of the pixels that were not correctly identified as background. From the tomograms the average density of the hair is calculated to be in the interval 1.17-1.29 g/cm^3. The smallest value of normalized absolute error δ obtained with DISRA was of 0.235. In [4] it is mentioned that, despite being a demanding criterion, values below 1% are reasonable. The large value obtained reflects the found experimental problems which required a correction of the projections that introduced artifacts.
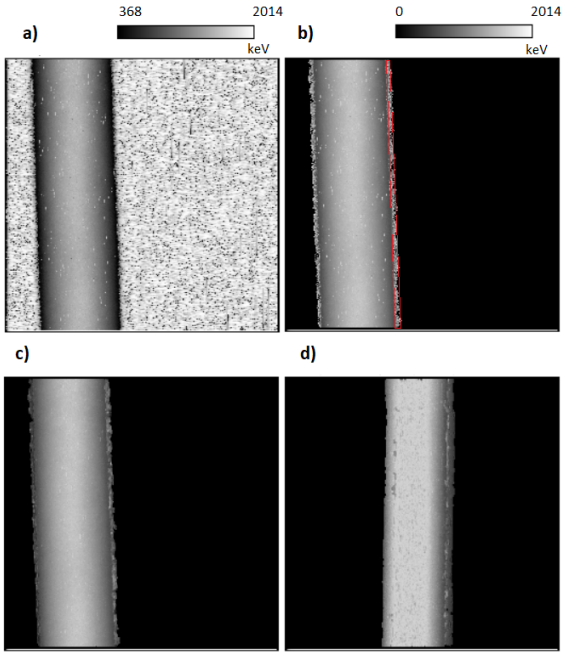
Figure 8: a) - energy loss map obtained at an angle of 60º after median filtering using the energy interval [330 keV, 1640 keV]. b) - the same map as in a) but with the background pixels identified and corrected. Some pixels near the borders of the sample were not corrected. The ones at the right side of the sample are indicated in red. c) - the map in b) after using the algorithm for the correction of spurious pixels described in 3.1.1. d) - result of the correction procedure on the energy loss map obtained at an angle of 162º.
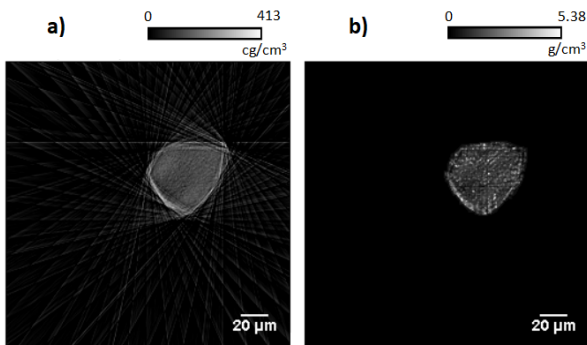

Figure 9: Tomogram of the slice number 143 out of 256. In a) the reconstruction was performed with TomoRebuild by the FBP algorithm with the ramp filter. In b) the reconstruction was performed with DisraSlice and the DISRA algorithm. A threshold of 0 cg/cm^3 was applied to the tomogram in a).
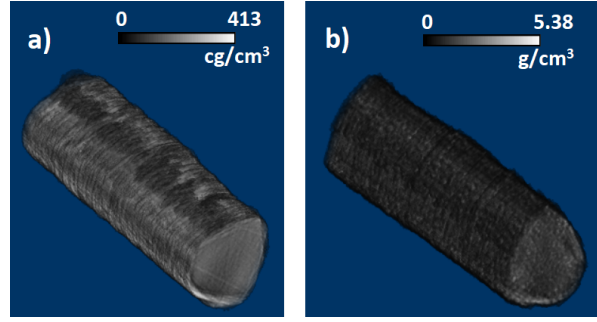

Figure 10: Three-dimensional tomogram of human hair. In a) the reconstruction was performed with TomoRebuild by the FBP algorithm with the ramp filter. In b) the reconstruction was performed with DisraSlice and the DISRA algorithm. Visualization made with ImageJ's plugin Volume viewer.

5. Conclusions

The main objectives of this work were to set the experimental equipment developed for STIM tomography again into operation and to automatize the data acquisition process. Regarding the automation the rotation of the stepper motor can now be executed with OMDAQ-3 (version 3.2.3.884) which allows for the sample to be rotated without the intervention of the operator. The high level of noise created by the current flowing in the motor when it is energized - which reached values of 3 V in the 0 V to 10 V range of the ADC used - was eliminated by suppressing the current before data is acquired. Electrical power is supplied to the motor only when it is about to move.

Despite the user not having to intervene in the rotation of the sample, a relative amount of attention must be dedicated to the experiment. The quality of the acquired data may not be satisfactory or the process may simply stop without the user's intervention. The latter situation happened (only) due to instabilities in the voltage produced by the Van de Graaff accelerator. If the voltage in the accelerator is not automatically reset in a way that the beam arrives at the experimental chamber in good conditions, this means that the projection under acquisition is lost and the process stops. This happened once during the analysis of the hair and once during the analysis of the pollen grain. The grain was left in the chamber and irradiated during the night but the process stopped with only half of the projections (15) complete. Even if the procedure does not stop the accelerator's voltage or the beam slits may need adjustment so that an appropriate rate of events is registered in the detector. The experimental system is complex and must be checked occasionally to make sure that none of its components is malfunctioning.

Since the manufacturer was made aware of this, it is expected that a new version of OMDAQ-3 will be available to correct for the bugs found. The most relevant one was responsible for the loss of the data of half of the projections (15) of the pollen grain, which was not saved during the acquisition. With a smaller importance it would be useful to correct the pixel clocking settings so that the number of counts per pixel are within a specified energy interval. This would provide a greater control over the quality of the data since electronic noise and pile up events would not be included in the counts.

The height of the sample must be appropriate for the incidence of the beam. Currently this positioning is made outside the chamber using millimeter paper with a reference mark that shows the correct position. If the adjustment is not made correctly this is noticed, naturally, after setting all the equipment on the target chamber with the sample properly positioned for the rotation. Removing the sample means removing all of this equipment and repeating the procedure not only for the adjustment of the height but also for the alignment of the rotation axis. This could be prevented if the operator could control the height of the sample in the target chamber. In the current configuration the goniometer that holds the sample is supported by a metallic basis that rests in the bottom of the target chamber. Since the goniometer cannot be moved without moving the basis a possible solution to this problem would be to have the whole set suspended and moved vertically by a set of motors with a resolution of a few micrometers.

JPIXET is now able to perform simulations on a new phantom with complex characteristics. This can prove to be useful for testing algorithms for STIMT reconstruction. The experimental parameters are provided through a set of files. The number of projections, the angular range, the energy and the dimensions of the beam can all be set by the user. For this functionality to be used in the future it would only be necessary to write the code that converts the file format produced by JPIXET - a binary file with the values of energy loss in MeV, one float for each pixel - in the format taken as input by the program in question.

Lastly it should be noted that the performed automation was the first one done, regarding the movement of the sample, on the microprobe at CTN. Many other techniques in which the sample is moved can benefit from the work performed. The DLL's compilation code can easily be adapted to other motorized stages with different degrees of freedom: up to 3 translation axes and up to 3 rotation axis.

References

[1] Ana Marques. Projecto microssonda 3d: tomografia por feixe de iões, Visitado a 10 de Setembro, 2020. `http://www.se.ctn.tecnico.ulisboa.pt/FisNuclear/MicroTomo3D`.

[2] A. C. Marques, M. M.F.R. Fraga, P. Fonte, D. G. Beasley, C. Cruz, L. C. Alves, and R. C. Da Silva. Performance of a gas flow ionization detector filled with He-iso-C_4H_{10} mixtures for STIM-T. *Nuclear Instruments and Methods in Physics Research, Section B: Beam Interactions with Materials and Atoms*, 348:100–105, 2015.

[3] D. G. Beasley, A. C. Marques, L. C. Alves, and R. C. Da Silva. Fast simulation of Proton Induced X-Ray Emission Tomography using CUDA. *Nuclear Instruments and Methods in Physics Research, Section B: Beam Interactions with Materials and Atoms*, 306:109–112, 2013.

[4] Arthur Sakellariou. *STIM and PIXE Tomography*. Phd, University of Melbourne, 2002.

[5] J. F. Ziegler, J. P. Biersack, and U. Littmark. *The stopping and ranges of ions in matter*. Pergamon Press, New York, 1985.

[6] C. Habchi, N. Gordillo, S. Bourret, Ph Barberet, C. Jovet, Ph Moretto, and H. Seznec. Beyond filtered backprojection: A reconstruction software package for ion beam microtomography data. *Nuclear Instruments and Methods in Physics Research, Section B: Beam Interactions with Materials and Atoms*, 295:42–49, 2013.

[7] Faycal Kharfi. Mathematics and Physics of Computed Tomography (CT): Demonstrations and Practical Examples. *Imaging and Radioanalytical Techniques in Interdisciplinary Research - Fundamentals and Cutting Edge Applications*, pages 92–95, 2013.

[8] Teunis van Beelen. Rs-232 for linux, freebsd and windows, 2020 (Visitado a 8 de Setembro, 2020). `https://www.teuniz.net/RS-232/index.html`.

[9] G.S. Kass and Lawrence M. Solomon. *Chemical and Physical Behavior of Human Hair*. Springer, Berlin, 5 edition, 2012.